Prediction and parametric analysis of cavity growth for the underground coal gasification project Thar

Article *in* Energy · February 2019

DOI: 10.1016/j.energy.2019.02.005

CITATIONS
17

READS
74

4 authors:

Syed Bilal Javed
National Engineering & Scientific Commission, Islamabad, Pakistan
11 PUBLICATIONS **47** CITATIONS
SEE PROFILE

Ali Arshad
COMSATS University Islamabad
39 PUBLICATIONS **364** CITATIONS
SEE PROFILE

Aamer Iqbal Bhatti
University of Engineering & Technology Lahore
245 PUBLICATIONS **2,091** CITATIONS
SEE PROFILE

Raza Samar
Capital University of Science & Technology
71 PUBLICATIONS **1,419** CITATIONS
SEE PROFILE

Prediction and Parametric Analysis of Cavity Growth for the Underground Coal Gasification Project Thar

Syed Bilal Javed[a], Ali Arshad Uppal[b], Aamer Iqbal Bhatti[a], Raza Samar[a]

[a] *Capital University of Science and Technology, Islamabad, Pakistan*
[b] *COMSATS University Islamabad, Pakistan*

Abstract

Underground coal gasification (UCG) is a promising clean coal technology to convert unmineable and deep coal reserves into syngas, which can be used in many industrial applications. In UCG field, real time monitoring of hydrological and geological conditions such as water influx rate, cavity growth and its interaction with overburden is a formidable task. UCG project Thar (UPT) lacks real time data acquisition system to monitor those parameters. In this work, a 3D axisymmetric cavity simulation model (CAVSIM) is parameterized with operating conditions of UPT and properties of Lignite B coal of Thar coal fields. For model validation with the UPT field data, a comparison has been made between the field and simulated data for the composition and heating value of syngas. The results of CAVSIM are also compared with our previous ID packed bed model, which show the superiority of CAVSIM model. Moreover, a comprehensive simulation study has been carried out to predict the cavity growth and its interaction with overburden. The effect of operating parameters of UPT on volumetric cavity growth and heating value of syngas are also investigated.

Keywords:
Underground coal gasification (UCG), Cavity growth, Energy conversion systems

1. Introduction

The world energy consumption will increase by 48% from the year 2012 to 2040 [1]. In 2040, the coal will contribute to almost 28% of the total

energy demand [1]. Fossil fuels currently account for over 85% of world energy consumption in which the contribution of coal is almost 28% [2]. The major advantages of coal over its counterparts like crude oil and natural gas are its relative abundance and low cost [3]. The coal deposits in Pakistan are about 185.17 billion tonnes [4], of which 175 billion tonnes of Lignite B coal is located in Thar desert [5].The major hindrance in the increased and continuous use of coal is its effect on environment [6, 7]. Therefore, clean coal technologies are opted to reduce the harmful effects of coal combustion on the environment [8–10]. The underground coal gasification (UCG) is one of the clean coal technologies, primarily used for low rank, un-minable and deeper coal seams [11, 12]. UCG in its most general form comprises of a pair of wells (inlet and outlet). The wells are linked by creating a permeable channel between them. A range of linking techniques have been reported in [13, 14]. The syngas produced by UCG can be burned to produce electricity, heat and can also be used in the manufacturing of chemicals such as ammonia and fertilizers [15].

UCG is viable for the Thar coal deposits due to the low rank nature of coal, variation in coal seam thickness and depths, loose formation and aquifers [16]. The planning commission of Pakistan has started the UCG project in Block V of Thar coal field sponsored by finance division [5]. Uppal et. al. [16, 17] developed a one-dimensional (1D) packed bed for the underground gasifier of UCG project Thar (UPT). The product gas composition and heating value were determined as a function of various operating conditions and coal properties. The results of the solved model were validated against the experimental data of UPT. The authors also implemented a constrained nonlinear optimization technique to optimize three stoichiometric coefficients of coal pyrolysis reaction. The parameter estimation was improved in [18], by formulating a relatively large scale optimization problem. Furthermore, in [18, 19] the authors designed different sliding mode controllers for maintaining desired heating value. The design of both the controllers is based on the model of [17].

1.1. Motivation and Related Work

In our earlier work [17], a one dimensional (1D) packed bed model of UCG was developed in which only the composition and heating value of syngas were determined as a function of the operating conditions of UPT and coal bed properties of Thar coal fields. In that model, energy and mass balances for the solids and gases were considered in one dimension only. Due

to the simplified geometry of the model, important multidimensional phenomena of cavity growth was not explained. Moreover, water influx was also assumed as a bounded disturbance. For any UCG site, the information about these parameters has paramount importance. The essential technical, environmental and economic feasibility analysis of a UCG field is based on the prediction of cavity growth [20–24]. Like other UCG fields, UPT has real time data acquisition system to measure the chemical process parameters such as composition, flow rate, pressure and temperature of injected and product gases. While UPT lacks such instrumentation resource to monitor the hydrological and geological conditions like water influx rate, cavity growth and its interaction with overburden. An intensive real time monitoring system is required to measure these process details, and the installation of such a monitoring system in itself is a challenging task. In [25], based on various UCG field trials reports of USA, it has been reported that there is not a single method which can provide complete details about the real time evolution of cavity.

The major real time problem being faced at UPT was the sudden drop in heating value of product gas. After thorough analysis of literature and previous UPT tests, it was found out that the investigation of cavity growth is essential to determine the reason of above issue. But as discussed earlier, real time monitoring of the cavity evolution is not possible at the UPT site. Moreover, the excavation of burnt cavities and outflow channel has also not been performed so far at the UPT site. Hence, a detailed simulation study is required to address the aforesaid real time issues related with UPT field. The simulation studies already available in the literature are also not applicable to the UPT field, as the cavity growth itself is a function of the operating conditions and coal bed properties of any UCG site.

Numerous resource recovery models are developed to study the cavity growth in UCG [20, 24, 26–30]. Beizen et al. [26] applied the probabilistic simulation approach to develop an integrated 3D channel model for UCG. In this model, the mass transport and reactive heat effects were combined with the properties of thermo mechanical failure of overburden to study the evolution of cavity. This modeling method is not feasible for low rank coal seams, having high permeability. Najafi et al. [27] developed a simple empirical model based on nonlinear regression analysis. The proposed model was capable to predict the cavity growth rate for the given operating parameters of UCG site. This models does not account for the cavity shape, spalling of overburden and water influx rate. In [28, 29], authors proposed

a computational fluid dynamics (CFD) model to simulate the UCG process. The reaction kinetics, mass and heat transfer, permeability limits, and the spalling of coal due to thermo-mechanical failure were investigated in an integrated manner. This model is only applicable to laboratory scale UCG setup. Jowkar et al. [20] proposed a simple statistical model to predict the cavity shape and volume, based on data obtained from Daggupati et al. experiment [31]. This model is applicable to commercial scale only if the UCG site has similar coal bed properties and operating parameters as considered in initial experiment. The coal bed properties and operating parameters of UPT field have large disparity as compared to the parameters considered in that model. Thus, this model in not applicable to the UPT field.

Moreover, the parametric study of cavity growth rate is also very important for any UCG site. The sensitivity analysis of cavity growth rate to different coal bed properties and operating parameters of the UCG field has been reported by several investigations [21, 22, 32–35]. In [22, 32], the authors have investigated the dependency of cavity growth rate on various operating parameters and coal bed properties. The study revealed that the optimum operating conditions are necessary to obtain the maximum energy effectiveness and gas production. Daggupati et al. developed a UCG model to investigate the formation of cavity [33]. The effect of various operating conditions and process design parameters such as inlet gas flow rate, operation time and distance between the wells on cavity growth were also studied. In [34], authors have investigated the effect of coal bed properties and inlet gas composition and flow rate on the cavity growth rate. It was found that high flow rate of O_2 is necessary to ensure the cavity growth in all directions and it had significant effect on cavity growth. In [21, 35], Perkins studied the impact of operating parameters on the lateral cavity growth rate. The results showed that the operating pressure, oxygen injection rate and coal properties affect the lateral extent of cavity, which directly affects the cost of heating value of syngas.

Similarly, the research work in the area of UCG conducted at the Lawrence Livermore National Laboratory (LLNL), USA resulted in the development of CAVSIM and 3D UCG simulator (UCG-SIM3D) models [24, 30, 36]. These two models serve as a benchmark for a UCG process, and the sophisticated simulators of these models are also available. The essential chemistry, gas transport, heat transfer, water influx, spalling of overburden and coal, and accumulation of rubble within the cavity were considered in the formulation of CAVSIM. The major attribute of this model is that it was formulated

on the basis of understanding and analysis experienced during various field trials [25]. In UCGSIM3D, the phenomena similar to CAVSIM have been modeled. It is a complex model, providing few advances over the CAVSIM, like flexible 3D geometry, including multiple seams, and rock strata, dip, and spatially-varying properties of the geological materials.

Although UCGSIM3D provides few advances over CAVSIM but the sideward and upward growth of cavity in coal seam and overburden is considered by spalling in both CAVSIM and UCGSIM3D models. The development of UCGSIM3D ended prior to become a mature engineering tool for use by non-experts [25]. In contrary to CAVSIM, UCGSIM3D is a complex model, requires high computational platforms and also a very limited literature is available regarding the formulation of UCGSIM3D. One of the fundamental objectives of the current research is to develop a model-based control for UPT, with an intent to increase the efficiency of the UCG process. To employ model-based control, model selection plays an important role. Too complex model can complicate the task of control design. Therefore, CAVSIM is preferred over UCGSIM3D in this work.

1.2. Major Contributions

A number of UCG models have been reported in the literature [20, 24, 26–30], which are capable to predict cavity growth rate. However, the prediction of water influx rate is not available in these models. Most of these models have been applied at laboratory-scale for the prediction of cavity growth rate, but they are not being used at commercial scale. The essence of this work is to predict the details of those parameters at which there is no direct access at the UPT site, while they have key role in determining the overall performance of the UCG system.

In this work, CAVSIM is used to perform a detailed simulation study in order to address the aforesaid real time issue related with the UPT field. CAVSIM is parametrized with the operating conditions of UPT and properties of Lignite B coal of Thar coal fields. The model is validated with the field data of UPT by comparing the composition and heating value of the syngas. The results are also compared with our previous 1D packed bed model [17], which shows that the predictions of CAVSIM are better as compared to the previous model. Moreover, CAVSIM is used for the prediction of cavity growth and its interaction with overburden. It has been observed that the cavity growth impacts char production, water influx and produced

species flow rates and heating value of the product gas. Furthermore, the effect of operating parameters on the cavity growth and heating value are also studied, which can be helpful to improve the outcome of field trials conducted at UPT.

Rest of the paper is organized in the following manner. The description of model is given in Section (2). The experimental setup is depicted in Section (3). The parametrization and results of the model and field trials are compared in Section (4). The model predictions are discussed in Section (5). Section (6) explains the effect of operating parameters on cavity growth and heating value, and finally the paper is concluded in Section (7).

2. Model Description

CAVSIM is a generalized model which can simulate UCG process for wide range of coal and overburden compositions and stratigraphy [24, 37–45]. Almost any flow schedule and composition of injected gases can be used in this model. It is applicable to flat-seam subbituminous or low rank coals in which the oxidant injection point is considered at the bottom of coal seam. An axisymmetric cavity geometry about an injection point is assumed to simplify the 3D growth into 2D. Although all apparent geometrical and thermo-physical symmetries have been exploited to simplify the problem but it retains sufficient detail to depict the main factors contributing in the cavity growth. CAVSIM is applicable only to the non-swelling coal seams of modest thickness (6-9 m) lies at modest depths (lower than 152.4 m) [37]. Thar coal deposits have low rank nature of coal and large variation in coal seam thickness (0.3m to 42m) and depths (122m to 180m) [46, 47]. It has very low free swelling index range from 0 to 1.5 [46]. In UPT, the field test conducted for a coal seam at the depth of 144 m and having thickness about 7.62 m. It can be seen that these parameters are within the acceptable range of CAVSIM, hence this model can be used for the UPT field.

The model mechanistically calculates cavity surface recession rates from mass and energy balances, and it is capable to simulate the cavity growth for entire life of UCG. It also integrates the results of different but interacting submodels, describing dispersion of injected reactants in a rubble bed at the bottom of cavity, water influx from the coal aquifer, degradation of rubble-covered coal sidewalls due to thermal stress and chemical reactions, recession of cavity surfaces enclosing a void space in the upper cavity caused

by radiation-driven spalling and gasification, and calculates the growth of outflow channel.

The model considers four solids: wet and dry coal and char (carbon) and ash. The complexity of the model is reduced by lumping $CO_2 + H_2O$ and $CO + H_2$ into two pseudo species such that only five gas-phase species are considered: O_2, reactant agent $R = CO_2 + H_2O$, gasification product $P = CO + H_2$, CH_4 and inert I.

The chemical reactions considered in this model are shown in Table 1. The simplification of reaction chemistry is justified by taking the similar stoichiometry of reactions R_2 and R_3, and assuming that water-gas shift reaction (R_4) is in equilibrium at cavity temperature. Therefore, the relative amounts of CO_2 and H_2 can adjust instantaneously to the local thermal environment. In this model, the reaction rates of $CO_2 + C$ and $H_2O + C$ are taken similar, and the heat of reaction of R_2 is defined in terms of inlet gas composition. The interacting submodels and global cavity simulator model are briefly described in the following sub-sections.

2.1. Water Influx Submodel

This model accounts for the flow rate of water in a UCG reactor. In UCG reactor, water can influx by various ways: injection of steam from the surface, drying and thermal decomposition of coal and rock, and flow of free water from the surrounding aquifers. The water entering due to drying and thermal decomposition of coal and rock is accounted by treating recession of these surfaces, injected steam is prescribed by the steam flow rate in the model and free water influx is computed by a simple model of saturated and unsaturated flow in the coal seam. The free water influx is assumed homogeneous and determined by two mechanisms: gravity drainage and pressurizing the coal seam [24, 42].

The problem of computing gravity drainage of water is simplified by using Dupuit approximation which assumed that volumetric flux of water across any vertical plane can be approximated as [51].

$$F_{v_W} = -K\frac{dh}{dr}. \tag{1}$$

The dimensionless form of surface height (h) is determined by using Eq.(1)

Table 1: Chemical kinetics for cavity growth

$R_1 : O_2 + C \rightarrow CO_2$
$\Delta H^o = -393.51(kJ/mol), \quad \Delta G^o = -394.36(kJ/mol)$
Reaction rate $(mol/m^3.s)$ [48]:
$k_r(c_T - c_{eq})$, where, $k_r = A\exp^{-E/RT}$
$R_2 : CO_2 + H_2O + 2C \rightarrow 3CO + H_2$
$\Delta H^o = 303.5(kJ/mol), \quad \Delta G^o = 211.5(kJ/mol)$
Reaction rate $(mol/m^3.s)$ [48]:
$k_r(c_T - c_{eq})$, where, $k_r = A\exp^{-E/RT}$
$R_3 : O_2 + CO + H_2 \rightarrow CO_2 + H_2O$
$\Delta H^o = -524.8(kJ/mol), \quad \Delta G^o = -485.8(kJ/mol)$
Reaction rate $(mol/m^3.s)$ [49]:
$4.75 * 10^5 [CO][H_2O] \left[\frac{17.5 * \frac{[O_2]}{c_T}}{1+24.7 * \frac{[O_2]}{c_T}}\right] \exp(-8050/T)$
$R_4 : H_2O + CO \rightleftharpoons H_2 + CO_2$
$\Delta H^o = +41.2(kJ/mol), \quad \Delta G^o = -28.62(kJ/mol)$
Reaction rate $(mol/m^3.s)$ [50]:
$568RT\left(0.5 - \frac{P}{2.53*10^7}\right)([CO] - [CO]_{eq})\exp\left(-13971/T\right)$

and applying conservation of mass.

$$\nabla.(h\nabla h) = \frac{\partial h}{\partial t}, \tag{2}$$
$$h = 1, \quad \text{for} \quad r \geq r_0(0), \quad \text{and} \quad t = 0,$$
$$h = 0, \quad \text{for} \quad r = r_0(t), \quad \text{and} \quad t \geq 0,$$
$$h \rightarrow 1, \quad \text{for} \quad r \rightarrow \infty, \quad \text{and} \quad t \geq 0.$$

Eq. (2) along with initial and boundary conditions is solved numerically by finite difference method using standard Livermore solver for ordinary differential equations (LSODE) [52]. The de-pressurization mechanism is in-

cluded in the Dupuit formulation by matching the drainage solution of Eq.(2) for the unsaturated and fully saturated region.

2.2. Flow Submodel

This submodel calculates the flow of injected gases through the distinct regions of ash rubble boundary. The boundary of ash pile is defined as: wall (ash–coal interface), the outer bed (char–ash rubble interface) and the inner bed (ash–void or ash–rock rubble interface). The model is based on the assumption that a region between the rubble and cavity wall is highly permeable relative to the rubble [24, 40]. The flow distribution is found by solving compressible form of Darcy's law, represented in cylindrical coordinates as:

$$\begin{aligned} \frac{\partial^2 P^2}{\partial z^2} + \frac{1}{r}\frac{\partial}{\partial r}(r\frac{\partial P^2}{\partial r}) + \frac{2RT\Omega\mu}{\kappa} = 0, \\ \frac{\partial P^2}{\partial z^2}|_z = \frac{\partial P^2}{\partial r^2}|_r = 0, \quad P^2(r = \psi(z,t)) = {P^2}_{sink}, \end{aligned} \tag{3}$$

where Ω represents the source strength of injection flow, which is nonzero only at the origin. A finite difference algorithm is used to discretize Eq.3 at each node, and then pressure at every node is computed by direct solution of the linear system in P^2.

2.3. Wall Submodel

A thin, highly permeable wall layer of thickness (δ) is assumed to exist between the ash pile and coal wall. This layer is filled by char and moves from left to right at a calculated speed, driven by thermally-induced rubblization of the coal wall on the right. The wall recession rate is determined by the heat flux which causes break down of wall into rubble [24, 40, 43, 44]. The relationship between temperature (T_ω) and recession rate (v) of wall layer is obtained by the balancing of net energy around a wall segment j.

$$\hat{Q}_{ox} = \hat{Q}_{dry} + \hat{Q}_{g_f} + \hat{Q}_{H_2O} + \hat{Q}_{redp_{j-1}} + \hat{Q}_{ch}. \tag{4}$$

Eq. 4 can be written as:

$$\begin{aligned} &F_{inj}\left[m_{O_2}q_3 - C_g(T_\omega - T_{inj})\right] = V\rho_{\mathbf{c}}\hat{Q}_{\mathbf{c}} + [F_{ch}W_{\mathbf{c}} + V\rho_{\mathbf{c}}W_{\mathbf{c}}]\frac{q_2}{M_{\mathbf{c}}} + \\ &F_{H_2O}\hat{Q}_{H_2O} + F_{p_{j-1}}C_g(T_\omega - T_{\omega_{j-1}}) + F_{ch}W_aC_s(T_{inj} - T_\omega). \end{aligned} \tag{5}$$

The expression of convective heat transfer from the product gas to the cold coal wall relates the recession rate and reaction zone temperatures [43, 44].

The δ in terms of T_ω is given by rearranging the equations given in [43, 44].

$$\delta = \left[\frac{x_1 P_r^{1/3} \lambda_g}{U d_p} \left(\frac{F_p d_p M_g}{\mu_g} \right)^{x_2} \times \frac{\ln\left(1 + \frac{T_\omega - T_f}{T^* + T_f - T_v}\right)}{F_{H_2O} C_g + \rho_{\mathbf{c}} V [W_{H_2O} C_g + (1 - W_{H_2O}) C_s]} \right]^{x_3}. \quad (6)$$

The mass balances around each segment give the product gas composition and flow rate as a function of injected gas rate and T_ω of segment. The effective extinction temperature (T_e) of the steam–char reaction in a packed bed is used to determine T_ω [45]. The solution of wall layer model is based on the assumption that gasification reactions quickly utilize the heat produced by oxidation reaction, such that product gas exits the segment at T_e.

2.4. Roof Rubble Submodel

The behavior of coal, char and rock ruble pile surfaces around the void region of cavity is described in the model. The model is based on the assumption that sidewall material and roof spalling are major parameters in determining the behavior of surface. When rock surfaces and coal are exposed to high temperature, spalling of material occurs due to thermally induced stresses. The heat transport from hot rubble bed surface to the spalling rock and coal surface, enclosing the void space is accounted by radiant heat [24, 40, 45].

The dynamics of char bed are described by assuming 1D packed bed model. The product gas composition, flow rate and carbon conversion rates are derived as a function of temperature T_e. The molar fraction of product gas is given below:

$$m_p = 2\frac{T_e}{T_{inj}} \left[\frac{1 - \frac{M_{\mathbf{c}} C_s m_{O_2}}{C_g W_{\mathbf{c}}} - \frac{q_1 m_{O_2} T_{inj}}{C_g (T_e - T_{inj}) T_e}}{\frac{M_{\mathbf{c}} C_s T_e (1 - m_{O_2})}{T_{inj} C_g W_{\mathbf{c}}} - \frac{q_2 + q_1 m_{O_2}}{C_g (T_e - T_{inj})}} \right]. \quad (7)$$

The product gas flux and carbon conversion rate are given by

$$F_p = \frac{2F_{inj}}{2 - m_p}. \quad (8)$$

$$r_c = F_{inj} \left(m_{O_2} + \frac{m_p}{2 - m_p} \right). \quad (9)$$

The system is solved by an efficient modification to Newton's method in which the inverse Jacobian Matrix is calculated [53].

2.5. Outflow Channel Submodel

In this submodel, the interaction of product gas which dries, pyrolyzes and rubblizes the coal surrounding the bore-hole is estimated. This submodel is not effectively coupled with main cavity model in a way that its presence does not affect the cavity growth, which means there is no feedback from channel to the cavity. This submodel combines all the gas source terms to determine the composition and temperature of a product gas leaving the cavity. It determines the flow rate of produced gas species individually from the lumped species by using carbon balances and invoking water-gas-shift equilibrium. The amount of coal pyrolysis and material balances give the amount of hydrocarbon (CH_4) and inert gas (N_2), respectively.

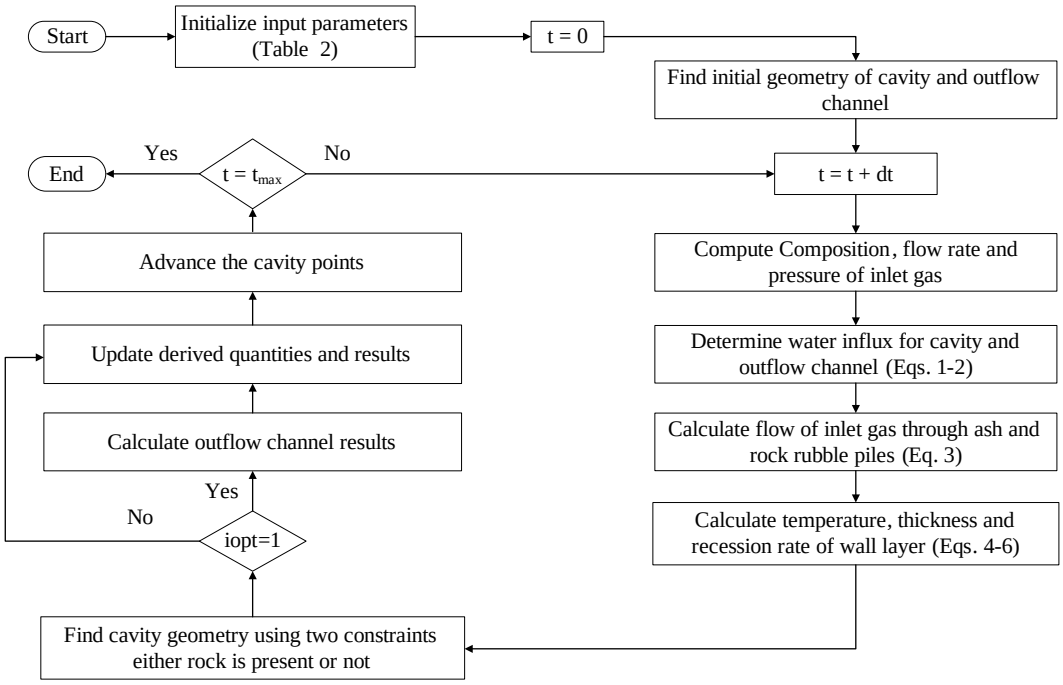

Figure 1: Solution routine of CAVSIM [24]

2.6. Cavity Growth Module

It is the main module which obtains the results of submodels described above and used them to calculate the boundaries of ash, char and rock rubble pile. Initially, half of a right circular cylinder is used to define the cavity geometry. It is divided into series of segments by points equally spaced along

the boundary. An initial size of char rubble pile is also specified. The submodels described previously, use the geometrical data to calculate recession rates, temperatures and rates of chemical reactions for different surface segments. This module uses a control segment to find the new location of cavity points, and computes tentative cavity boundaries and amounts of rubble. A distinctive shape of cavity is determined by considering different situations like, whether the cavity is interacting with overburden rock or it is confined in the coal seam. The solution routine of CAVSIM is briefly described in Fig. 1.

3. Experimental Setup

The important components of UPT experimental setup include UCG field, compressors, gas analyzer and control room. The schematic of the process is shown in Fig. 2.

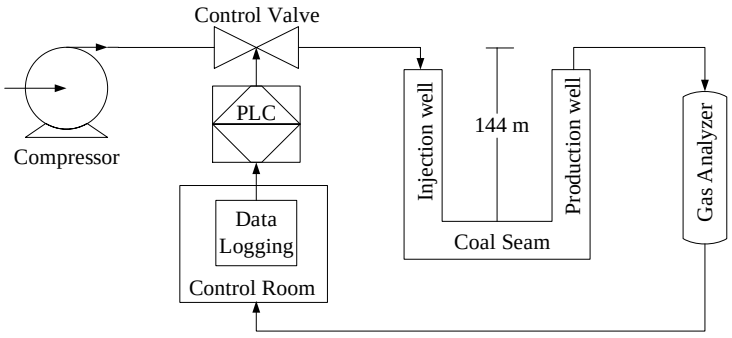

Figure 2: Process schematic diagram

Fig. 3 shows the UCG field, which is comprised of a network of pipes and wells, spanning an area of 18750 m^2. There are many UCG design concepts, which are mainly classified on the basis of drilling methods, placement of process wells and their linking techniques [22]. Linked vertically wells technique is used in the design of UPT field.

In a single gasifier, a pair of injection and production wells is necessary. The purpose of injection well is to supply compressed oxidants to the coal seam while production well transports the product gas to the gas analyzer. Air at a specific flow rate and pressure is supplied to the injection well through blue pipes, while the red pipes carry syngas from the production well to the gas analyzer. In a commercial UCG process, a number of coal seams are

gasified concurrently, therefore, having multiple production wells to recover the product gas. However, this experiment was conducted for a single coal seam located at the depth of 144 m from the surface.

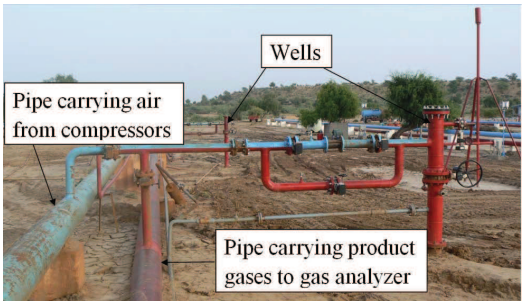

Figure 3: Field area of UPT. [17]

The permeability of coal seam is low, therefore, the reverse combustion linking (RCL) technique is used to establish a permeable channel between the wells. In RCL, oxidants are injected in one well while coal seam is ignited from other well. The idea is to establish low hydraulic resistance path between the wells by propagating combustion front towards the oxidant source. During the link establishment, air is supplied to the coal seam through the high pressure compressors. The low pressure compressors are used to supply air to the already ignited coal seam during gasification process.

The flow rate of injected air is set by the opening position of the control valve. The percentage opening of the control valve is controlled by the PLCs. The product gases are sent to the gas analyzer after removing steam. The coal gas analyzer [54] is used to measure the molar fraction of syngas and then heating value of gas mixture is calculated. A dual beam non dispersive infrared (NDIR) detectors are used to measure the molar fraction of CO_2, CO, CH_4 and C_nH_m. The molar fraction of O_2 and H_2 are measured by galvanic fuel cell and thermal conductivity detector (TCD), respectively. While the molar fraction of N_2 is calculated by using the measured values of other gases. The heating value of syngas is determined by Eq. 10.

$$HV_e = m_{CO_e} H_{CO} + m_{CH_{4_e}} H_{CH_4} + m_{H_{2_e}} H_{H_2} + m_{C_n H_{m_e}} H_{C_n H_m}, \tag{10}$$

where HV_e represents the experimental heating value of syngas (KJ/m^3), H_i and m_{i_e} are the heat of combustion (KJ/m^3) and experimental molar fraction percentage of syngas component i, respectively.

3.1. Assessment of Groundwater Contamination

The contamination of ground water is a major environmental concern related with any UCG site [25, 36]. The contamination of portable water aquifer is not possible at the UPT site due to its geological conditions. In Thar coal block-V, two aquifers are present above the coal seam and one is underneath the coal seams. According to Litho-log of well bore, these aquifers lie at average depth of 55-59m, 105-109m and 195-250m, respectively. The depth and thickness of coal seam ranges from 122m to 180m and 0.3m to 42m, respectively [46, 47]. The dug wells are being used to meet the drinking water requirements of local community, which relies on the first aquifer. The portable water aquifer cannot be contaminated in the UPT field area, as it is 100m above the area of UCG reactor. The second aquifer is also in the safe range of height [55]. The quality of second and third water aquifers are not suitable for drinking, as they have TDS range of 6000-10000 ppm that is brackish water and they are exempted from drinking regulation of EPA. The risk of contamination was eliminated by adopting the controlled operational practices during the test burn. Water samples from the UCG Grid area and dug wells of local community were collected regularly and tested for the organic pollutants like Ethyl Benzene, Phenol, Toluene, Benzene, and Xylene. All the parameters are within the safe limit of WHO for drinking water guidance [55].

4. Model Validation

The simulation results of CAVSIM have been validated with the field trials carried out at UPT. The details of parametrization and comparison of simulated and experimental data are given in the following subsections.

4.1. Model Parametrization

The process of UCG is sensitive to the operating conditions and coal bed properties. The operating conditions include composition, temperature, pressure and flow schedule of injected gas mixture. The parametrization of CAVSIM has been carried out by the data obtained from UPT. The detail of the parameters is given in Table 2.

Table 2: Parameters used in simulation

Parameters		**Values**
Solid	Coal Type	Lignite B
	Density of Coal (kg/m^3)	1250
	Molecular weight of Coal (kg/mol)	0.02
	Initial particle diameter (m)	0.01
	Adjacent coal open or flow porosity	0.005
	Coal Permeability (m^2)	$1.97e^{-13}$
	Ash Permeability (m^2)	$2.96e^{-12}$
	Rock Permeability (m^2)	$2.96e^{-12}$
	Coal weight fraction	0.2822
	Ash weight fraction	0.1892
	Moisture weight fraction	0.3682
	Volatile Matter	0.3824
	Heat capacity ($J/kg/K$)	1650
	Constant thermal conductivity ($w/m/K$)	1.0
	Coal failure temperature (K)	700
	Coal roof failure length (m)	0.01
Gas	Composition of injected gas	Dry air
	Injection flow (mol/s)	Actual UPT field data
	Pressure of gas at the inlet (Pa)	6.18e+6
	Temperature of gas at the inlet (K)	430
	Ambient temperature (K)	285
	Steam temperature (K)	373
	Heat source temperature (K)	1000
	Constant roof temperature (K)	1000
	Viscosity functions ($kg/m/s$)	$4.0e^{-}6, 2.93e^{-}8$
	Heat capacity ($J/mol/K$)	45
	Pyrolysis gas molecular weight (kg/mol)	0.02
Cavity	Initial cavity geometry	Right circular cylinder
	Initial cavity height and radius (m)	3.62, 1.82
	Cavity pressure (Pa)	3.05e+5

4.2. Results Comparison

The simulations are performed for 1.5 days with a step size of an hour to compare the experimental and simulated results. Air is used as an oxidizing agent. The time profile of air flow rate is shown in Fig. 4. In Fig. 5, the composition and heating value of syngas predicted by CAVSIM and by 1D packed bed model [17] are compared with the UPT field data. It can be seen that the CAVSIM predictions are much better than the results produced by [17]. In Table 3, the relative errors (*Eq.*(11)) of field data (y_{exp}) and simulation results (y_{sim}) are shown for both models.

$$\|e_{rel}\|_2 = \frac{\|y_{sim} - y_{exp}\|_2}{\|y_{exp}\|_2}. \tag{11}$$

Therefore, a comprehensive simulation study is carried out in the subsequent sections to predict the cavity growth and its impact on the UCG process. Furthermore, the effect of operating parameters on cavity growth and heating value of product gas are also studied.

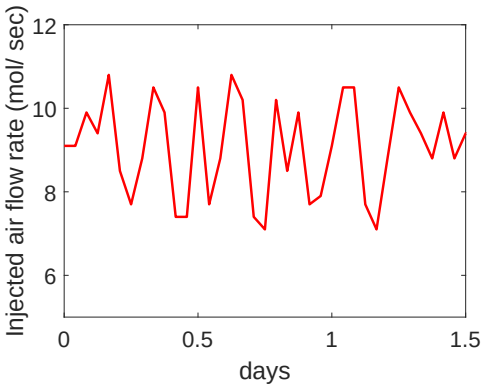

Figure 4: Flow rate of injected air

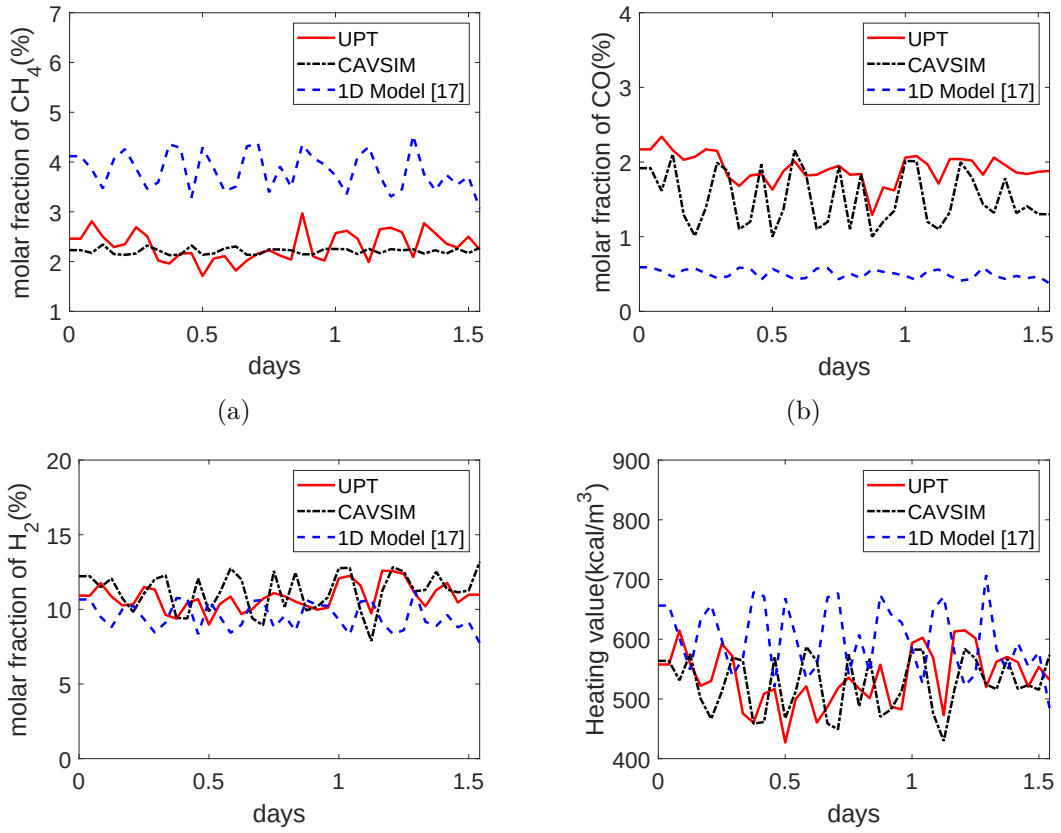

Figure 5: Model validation: (a-c) Molar Fraction of Syngas Species with Time, (d) heating value of syngas

Table 3: Relative error for field and predictions of models

Parameter	**% Relative error (CAVSIM)**	**% Relative error (1D Model[17])**
CH_4	13.67	68.39
CO	26.23	74.44
H_2	9.12	14.59
Heating value	9.49	20.13

5. Model Predictions

In this section, CAVSIM is used to predict the important UCG phenomena for UPT field trials. The simulations are performed to predict the cavity growth and its interaction with the overburden. Moreover, the effect of cavity growth on char production, water influx and produced species flow rates, molar fraction and heating value of the product gas are studied.

The simulations are performed for 45 days to investigate the evolution of cavity in UPT field. Fig. 6 shows the prediction results of cavity growth at various stages of the process. The flow rate of injected air reaches a distinct region of the cavity as shown in Fig. 7. The geometry of rubble region is characterized with points a, b, c and d, as show in Fig. 6. It can be seen that different points are coincident in time due to appearing and disappearing of various rabble materials. The top of ash pile is defined by points b and c, and angle γ of line which joins these points. This angle is used to approximate a somewhat rounded ash rubble pile. The char pile top is defined by points a, d and the top of rock rubble is defined by point a. The line between points a and d makes an angle ω, which is a model parameter used to represent the angle of repose of char rubble. The wall region is defined as the cavity boundary extending downward to the bottom of cavity from point c. The material balances and angles γ and ω are used to determine the location and evolution of these points.

The rubble pile top (rubble–void interface) is divided into outer and inner bed, represented by points a, d and a, b, respectively, as shown in Fig. 6(d). The char accumulates onto the outer bed due to spalling of roof and rubblization of adjacent coal side wall. The rubblization of wall takes place in accordance to the heat transfer mechanism, explained in section (2.3) [24]. The outer bed loses char due to the number of factors which include: reaction with injected gases, fraction of char rolls off onto the inner bed where it is consumed by reaction and settling of char along the wall zone.

The inner bed is in the middle of rubble surface where no net char accumulation is allowed. There exists a condition that either char is present in a thin quasi-steady layer or not in the inner bed. When enough amount of char is present in this region to consume all the injected O_2, the endothermic gasification reaction is balanced with the heat loss from the bed by radiation. This balance determines the ultimate composition of product gas and temperature reaching the void. Contrarily, for the insufficient char, it is assumed that void space is well-mixed such that gas species 'P' in a void space

react with excess O_2, which causes heat radiation to the remaining surfaces enclosing the void.

The cavity geometry is initially assumed as a right circular cylinder with radius, r = 1.82m and height, z = 3.62m. The initial cavity shown in Fig. 6a is rectangular due to the assumption of axisymmetric cavity growth around the injection point which simplifies the 3D growth into 2D. The cavity shape for the situation when cavity lies within the coal seam is determined by taking into account the amount of char falling in the inner ash rubble surface, which determines the upward growth of that surface, distribution of temperature in the enclosure and amount of char left in the rubble bed. Thus, only one solution exists for the char appeared on ash–void interface represented by the position of point b in Fig. 6(b-c), which simultaneously satisfies both ash and char material balances. This solution is determined by performing iterations on α and use golden section algorithm. It is observed in Fig. 6(b-c) that the cavity grows smoothly in all directions and its rate of lateral and upward growth relatively remains constant when the cavity is confined to the coal seam. It is also observed that the amount of unburned char increases in proportion to the cavity volume.

When the cavity includes rock, it can be observed in Fig. 6(c-f) that the ash pile controls the injected gas flow distribution, stops to grow upward and its height becomes constant. Thus, the location of point b is determined by only the ash mass balance, while point a is fixed at a place where char and rock rubble material balances are simultaneously satisfied. Fig. 6e shows the situation when char region is completely covered by the rock rubble and represented by the coincidence of points a and d. Finally, the char depletion situation is described in Fig. 6f, where point b moves radially and coincides with point c at a constant height due to the char material balance.

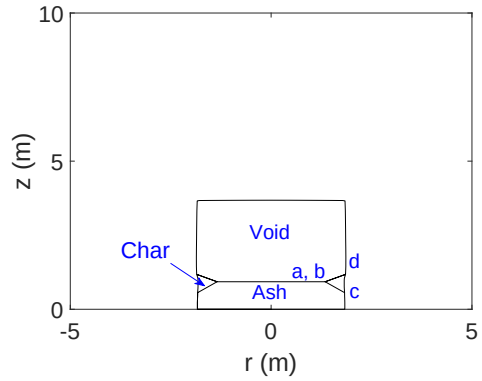

(a) **Initial cavity shape at** 2^{nd} **hour**, inlet air flow rate (mol/s) = 17.09, produced char/ O_2 (mol/mol) = 1.41, $(H_2 + CO)/O_2$ (mol/mol) = 0.82

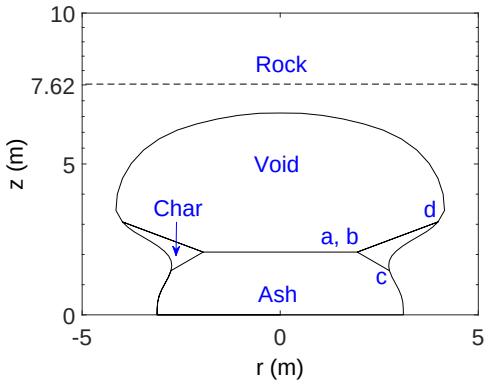

(b) **Cavity shape at** 20^{th} **day**, inlet air flow rate (mol/s) = 9.2, produced char/ O_2 (mol/mol) = 1.24, $(H_2 + CO)/O_2$ (mol/mol) = 0.53

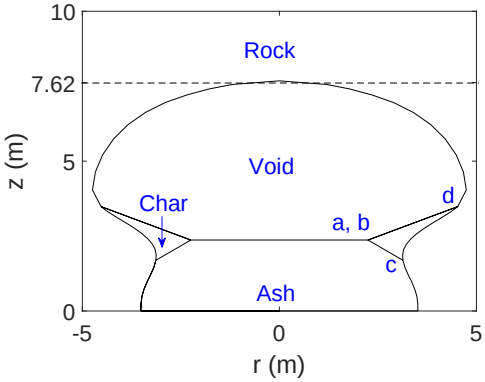

(c) **Cavity shape at** 34^{th} **day**, inlet air flow rate (mol/s) = 9.2, produced char/ O_2 (mol/mol) = 1.258, $(H_2 + CO)/O_2$ (mol/mol) = 0.54

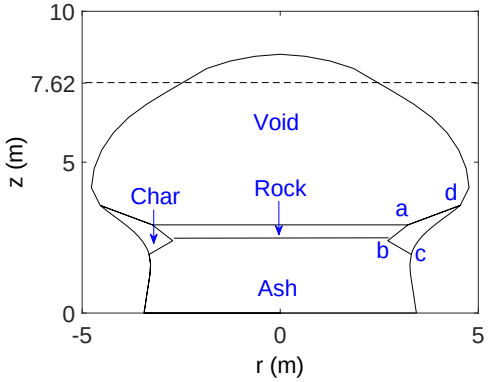

(d) **Cavity shape at** 36^{th} **day**, inlet air flow rate (mol/s) = 9.2, produced char/ O_2 (mol/mol) = 1.34, $(H_2 + CO)/O_2$ (mol/mol) = 0.68

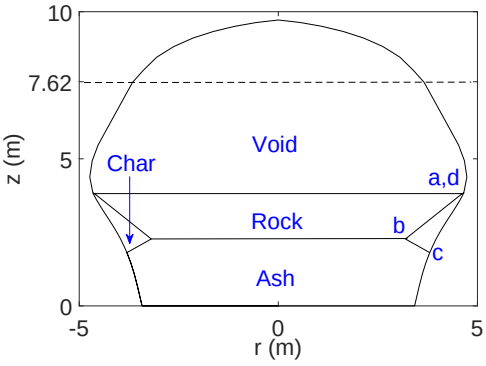

(e) **Cavity shape at** 40^{th} **day**, inlet air flow rate (mol/s) = 9.2, produced char/ O_2 (mol/mol) = 1.52, $(H_2 + CO)/O_2$ (mol/mol) = 1.01

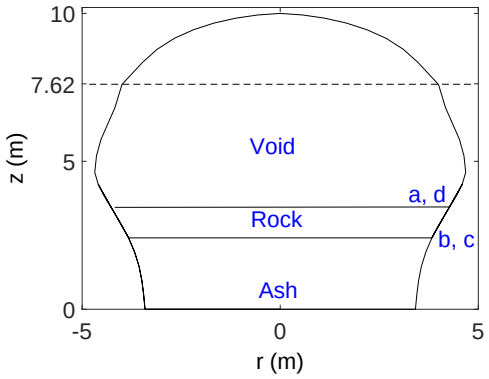

(f) **Cavity shape at** 45^{th} **day**, inlet air flow rate (mol/s) = 9.2, produced char/ O_2 (mol/mol) = 1.23, $(H_2 + CO)/O_2$ (mol/mol) = 0.2

Figure 6: Cavity shapes at various stages of UCG

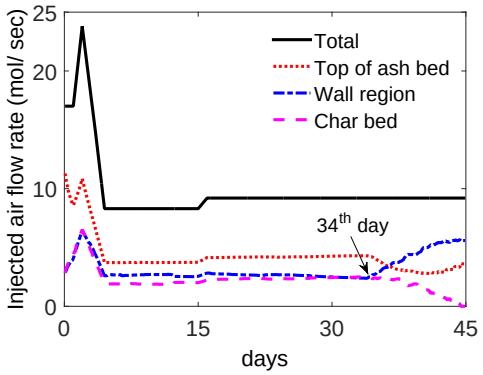

Figure 7: Flow rate of injected air

The molar ratios of produced char and produced gas ($P = CO + H_2$) to the rate of injected O_2 is shown in Fig. 8, which are important quantities to measure the performance of gasifier. The behavior of molar ratios follow the same trend as the rate of injected O_2 till 34^{th} day. In Fig. 8, the change in behavior of molar ratios near the 34^{th} day is due to the interaction of cavity with the overburden rock. When the overburden rock is included in the cavity, the flow rate of injected air increases towards the wall region as shown in Fig. 7. This increases the molar ratios of produced char and produced gas. It can be seen that the molar ratios decrease abruptly after 40^{th} day, as the char region is completely covered by the overburden and char begins to deplete from the cavity as discussed previously.

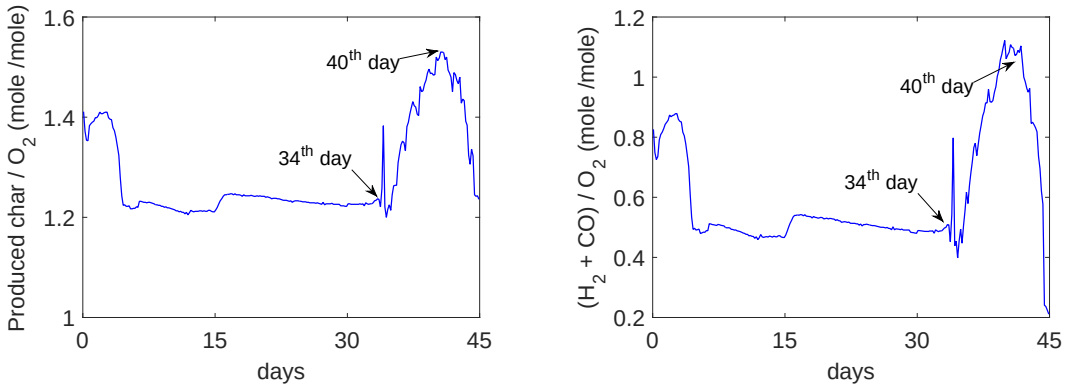

(a) (b)

Figure 8: Molar ratio of (a) produced char and (b) $CO + H_2$ per mole of injected O_2

The water influx rate, molar fraction, flow rate and heating value of produced species are shown in Fig. 9. The water influx rate of outflow channel is an important parameter in a real system. In Fig. 9a, the model predicts that the ratio of cavity and channel water influx begins with 1:1 at the early stage of simulations, and tends to be greater than 2:1 for mature cavity. It can be observed in Fig. 9a that rock water increases as the cavity interacts with overburden at 34^{th} day, which increases the total water influx rate. The increase in water influx favors steam gasification ($C + H_2O \rightarrow H_2 + CO$) and water gas shift reactions ($CO + H_2O \rightarrow H_2 + CO_2$), which increase the flow rate of H_2 and CO_2 as shown in Fig. 9b. However, the amount of CO remains constant as CO is acting as a reactant in the latter reaction. As the cavity grows further, char is completely covered by rock and begins to deplete at 40^{th} day, causing reduction in the flow rate of produced gas species. The molar fraction and heating value of the product gas have similar trends as the flow rate of gasification product ($H_2 + CO$) as shown in Fig. 9c and Fig. 9d, respectively. The decrease in flow rate, molar fraction and heating value of the product gas near the day 05 is observed, which is due to the lower injection rate of air, which can be seen in Fig. 7.

It can be seen that the deterioration in heating value of syngas is due to the interaction of cavity with overburden. In Fig. 9(a), it can be seen that total water influx begins to increase at 34^{th} day. At this time, cavity interacts with overburden as shown in 6c. The increase in water disrupted the operation of UCG gasifier and reduces its temperature. Therefore, the decrease in temperature results in the deterioration of heating value.

In this section we have seen that the major factors contributing in the UCG process are the function of cavity growth. Therefore, the prediction of cavity growth has significant role in determining the overall performance of UCG process. Thus, the parametric study is essential to improve the performance of UPT field.

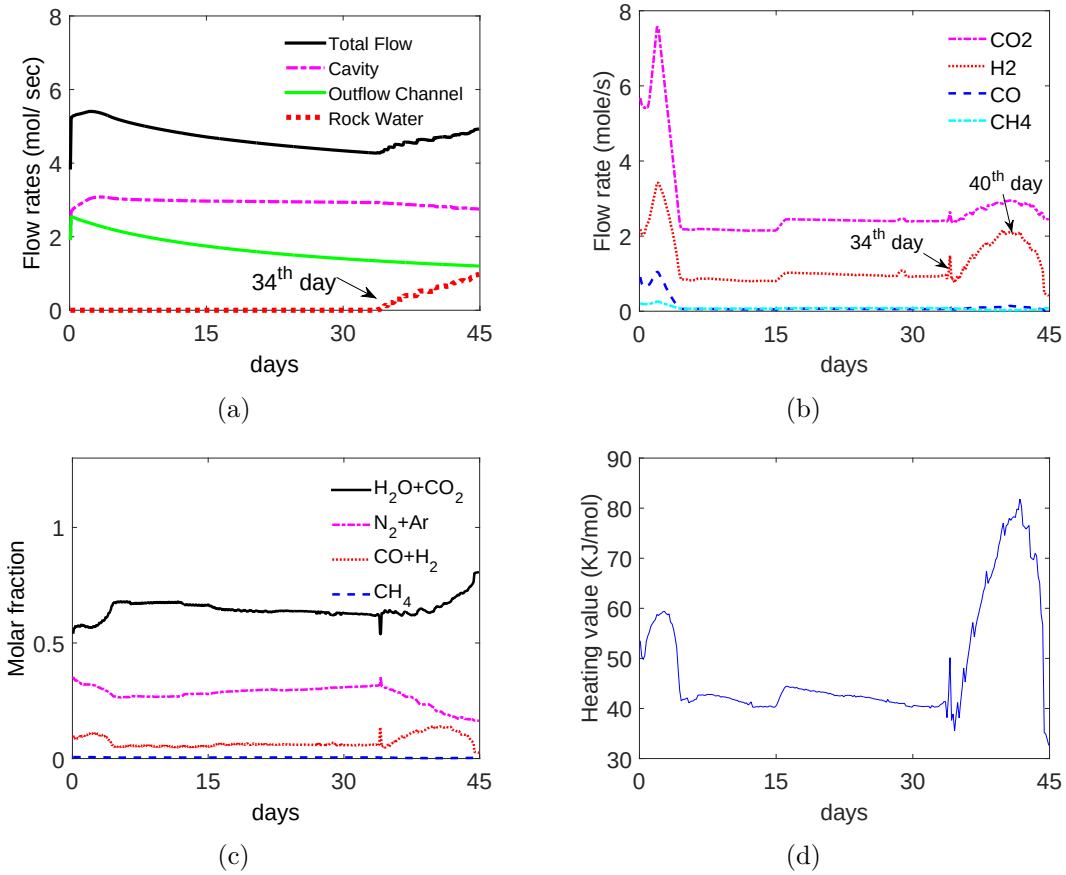

Figure 9: (a) Water influx rate, (b) produced species rate, (c) composition of product gas, (d) heating value of product gas

6. Effect of Operating Conditions on Cavity Growth

In this section, the effect of operating parameters of UPT field on the volumetric cavity growth and heating value of the product gas has been investigated. The effect of inlet gas composition, O_2 concentration, steam/O_2 ratio (α) and flow rate of injected gas are studied here.

6.1. Effect of inlet gas composition

The composition of injected gas is an important parameter in the UCG process. The details of inlet gas composition are given in Table 4. In Fig. 10a, it can be observed that the cavity growth rate is higher when the injected gas comprises of steam and O_2 instead of dry air. With the inclusion of steam in

the injected gas, the amount of N_2 reduces which causes an increase in the concentration of reactant gases. Thus, resulting in a high consumption rate of char. The heating value of product gas for various inlet gas compositions is

Table 4: Composition of Injected gas

Sr. No.	**Injected gas species**	**Mixture of steam and O_2**	**Dry air**
1.	O_2	20%	21%
2.	H_2O	60%	0
3.	N_2	20%	79%

compared in Fig. 10b. It can be seen that the mixture of steam and O_2 in the injected gas gives high heating value as compared to the dry air. The presence of steam in an inlet gas enhances the gasification reaction, resulting in a higher heating value of the product gas. The variation in heating value near the 10^{th} day is due to the cavity interaction with overburden, as explained in the previous section.

It has been shown that the composition of injected gas has significant effect on the heating value of product gas. The mixture of steam and O_2 is best suited to obtain high heating value from the UCG process. However, an optimum value of steam to O_2 ratio is required.

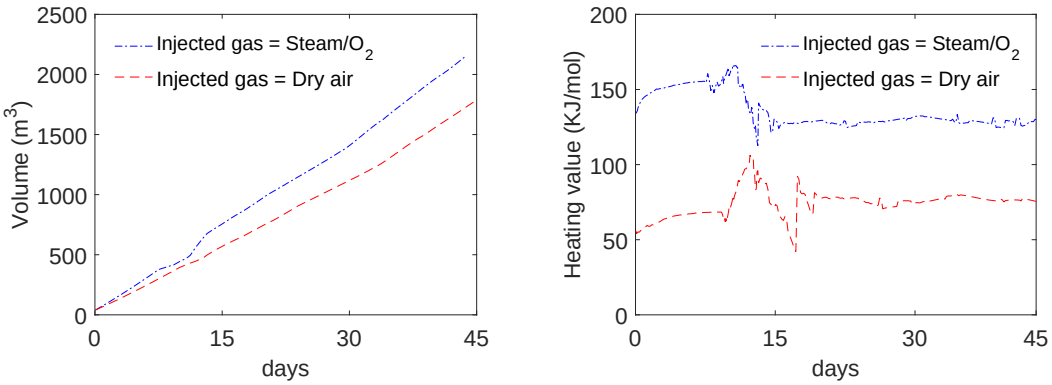

(a) Volumetric cavity growth rate

(b) Heating value

Figure 10: Effect of inlet gas composition

6.2. Effect of varying O_2 concentration

The effect of injected O_2 concentration with constant steam to oxygen ratio (α) on the volumetric cavity growth and heating value is explored here. The injected gas composition is shown in Table 5. The results are illustrated for three different cases in which concentration of O_2 is 25%, 20% and 15%, respectively. To keep α constant, the steam concentration is also varied in accordance with the amount of O_2.

The increase in concentration of O_2 increases the rate of exothermic oxidation reaction, which rises the temperature of the UCG reactor. Besides this, the amount of H_2O also increases, resulting in a higher concentration of reactants. With the increase in total amount of reactants, volumetric cavity growth is expected to increase, which is depicted in Fig. 11a. The rise in temperature along with the increased concentration of H_2O favors the endothermic gasification and water gas shift reactions, which increases the amount of CO and H_2. Moreover, it can be seen that with decrease in amount of N_2 which is an inert gas, the concentration of reactant gases: O_2 and H_2O increase. Therefore, the decrease in N_2 increases the chemical reactions within the UCG reactor, resulting in the higher heating value of syngas, cf. [16, 56–58]. Similarly, for lower O_2 concentration the coal conversion and heating value decrease. It can be seen that for the higher concentration of O_2, cavity reaches overburden rock more quickly. In Fig. 11b, the effect of cavity interaction with overburden is seen at almost 8^{th} day for case-I, while for the other cases it happens at 11^{th} and 16^{th} day, respectively.

Table 5: Injected gas composition (effect of O_2 concentration)

Sr. No.	**Injected gas species**	**Case-I**	**Case-II**	**Case-III**
1.	O_2	15%	20%	25%
2.	α	1	1	1
3.	H_2O	15%	20%	25%
4.	N_2	70%	60%	50%

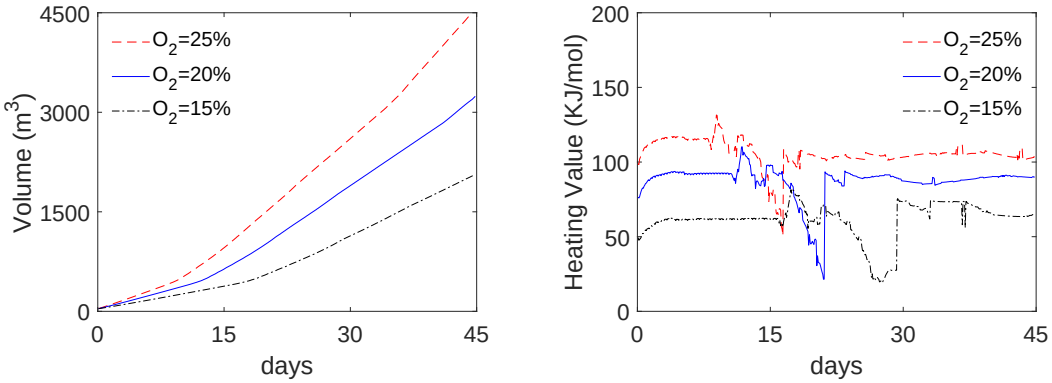

(a) Volumetric cavity growth rate

(b) Heating value

Figure 11: Effect of varying O_2 concentration

6.3. Effect of varying α

In this section, α is varied to investigate its effect on the volumetric cavity growth and heating value of the product gas. The variation in α can be carried out in two ways [59]:

- Keeping the inlet gas flow rate constant, and varying the amount of O_2 and H_2O in inlet gas, as shown in Table 6.
- The inlet gas flow rate and amount of O_2 are kept constant, and the amount of H_2O is varied only, as shown in Table 7.

Firstly, the analysis is performed for the former case. With the increase in α, concentration of O_2 decreases and amount of H_2O increases. As O_2 is decreased the temperature of the UCG reactor drops, which slows down the rate of endothermic gasification reactions. Hence, it reduces the coal consumption rate, which is shown in Fig. 12a. Subsequently, with the increase in α the heating value of syngas also reduces, as shown in Fig. 12b, cf. [56, 59].

Table 6: Composition of Injected gases (effect of α)

Sr. No.	Injected gas species	Case-I	Case-II	Case-III	Case-IV
1.	O_2	50%	40%	30%	20%
2.	H_2O	50%	60%	70%	80%
3.	N_2	0%	0%	0%	0%
4.	α	1	1.5	2.3	4

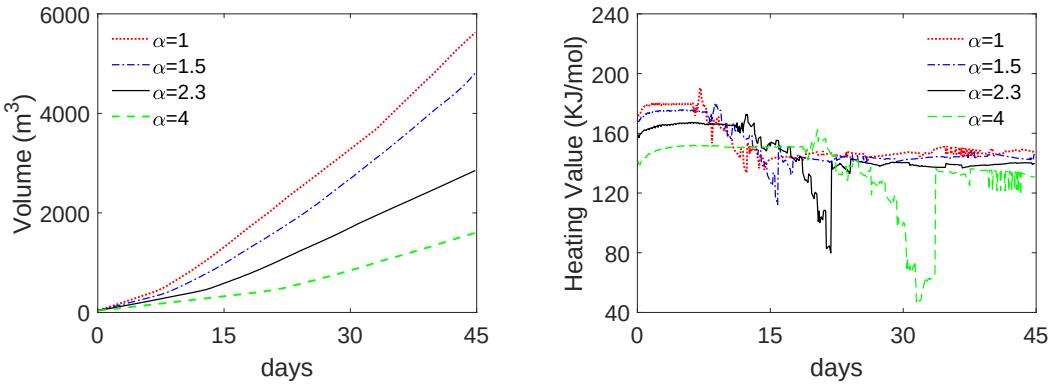

(a) Volumetric cavity growth rate

(b) Heating value

Figure 12: Effect of varying α

Now, the analysis is carried out for the second case in which α is varied by changing the amount of H_2O, while amount of O_2 and flow rate are kept constant. As the concentration of O_2 remains constant, therefore, the rate of oxidation reaction does not change. Which in turn maintains a constant temperature of the UCG reactor, therefore, the coal consumption rate is also constant, as shown in Fig. 13a. Moreover,the concentration of H_2O increases with the increase in α, which enhances the water gas shift and gasification reactions, resulting in a higher heating value as shown in Fig. 13b, cf. [16, 56, 59]. Moreover, it can also be seen that with the increase in concentration of N_2, the molar fractions of the reactant gases: O_2 and H_2O reduce. The decrease in the amount of reactant gases reduces the chemical reactions within the UCG reactor, resulting in the deterioration of the heating value as observed in Fig. 13b. It can also be seen that the cavity interacts with overburden at the same time for all the cases, due to constant coal consumption rate. It is pertinent to mention that the aforementioned phenomena hold for

the concentration of steam not exceeding a certain value.

In UCG, steam and O_2 both are the reactant agents and have key role in obtaining the desired heating value of the product gas. A certain amount of H_2O is required for the gasification reaction while on the other hand, excess steam drops the temperature of the reactor due to the endothermicity of the steam gasification reaction. Therefore, an optimal value of α must be chosen to obtain the desired heating value.

Table 7: Composition of Injected gases (effect of α)

Sr. No.	**Injected gas species**	**Case-I**	**Case-II**	**Case-III**
1.	O_2	15%	15%	15%
2.	H_2O	15%	30%	45%
3.	N_2	70%	55%	40%
4.	α	1	2	3

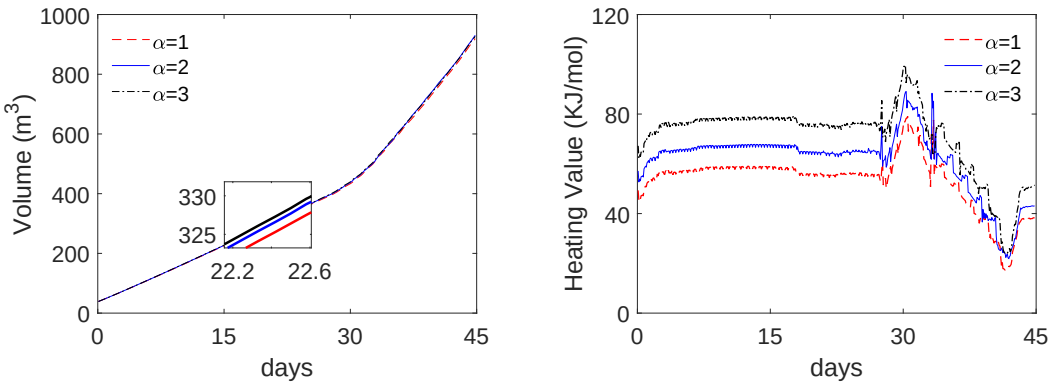

(a) Volumetric cavity growth rate

(b) Heating value

Figure 13: Effect of varying α

6.4. Effect of varying inlet gas flow rate

The evolution of cavity is also a function of the flow rate of injected gas. To study the effect of flow rate on cavity growth and heating value of product gas, the concentrations of $O_2 = 25\%$ and $\alpha = 3$ are kept constant. The results are discussed for different flow rates of inlet gas. Fig. 14 shows

that the volumetric cavity growth and heating value of the product gas are directly proportional to the inlet gas flow rate.

The above parametric study shows that the volumetric cavity growth and heating value of the product gas are sensitive to the operating conditions of UCG field. Thus, the operating parameters have vital role in determining the overall performance of UCG process. It can be concluded from the parametric studies that the optimal values of above mentioned operating parameters are required to obtain higher heating value of the product gas for a longer period of time.

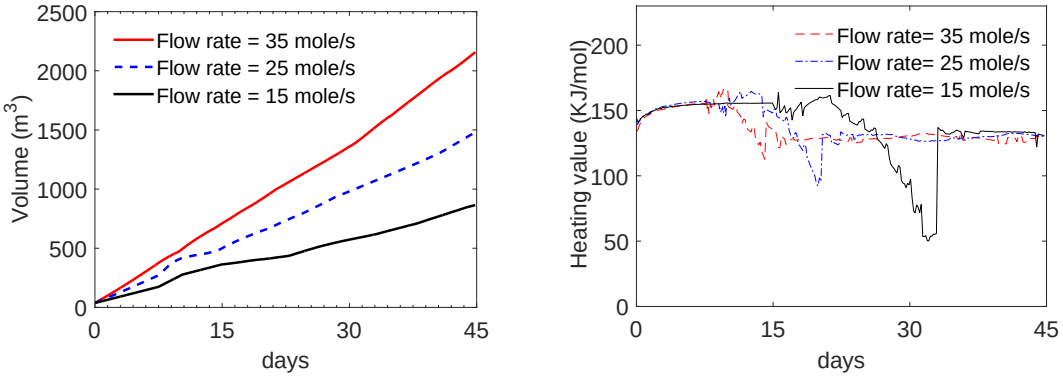

(a) Volumetric cavity growth rate (b) Heating value

Figure 14: Effect of varying inlet gas flow rate

7. Conclusion

In this work, CAVSIM has been parameterized with the operating parameters of UPT and the properties of Lignite B coal of Thar coal fields. The composition and heating value of syngas predicted by CAVSIM and 1D packed bed model have been compared with the field data of UPT. It has been shown that CAVSIM results are better and show a good match with the field data. The evolution of cavity at various stages of UCG process has also been explored. It has been observed that the essential UCG phenomena like char production, water influx and produced species flow rates and heating value of syngas are greatly affected by the cavity growth. Moreover, the simulation studies have been carried out to investigate the effect of various operating conditions on the volumetric cavity growth and heating value of the product gas. It is concluded that the volumetric cavity growth and heat-

ing value of the product gas are sensitive to the various operating parameters of UPT field.

The efficiency of a UCG process can be enhanced by designing a feedback controller, which optimizes the operating parameters. In future, CAVSIM can be employed for the model-based control of the UPT field.

8. Acknowledgment

The authors would like to thank the LLNL for providing CAVSIM. The authors also acknowledge UPT and control and signal processing research (CASPR) group at Capital University of Science and Technology, Islamabad for providing the technical assistance.

Nomenclature

Symbols

A	Pre-exponential rate constant $(1/s)$
C	Specific heat capacity $(J/kg.K)$ for solid, $(J/mol.K)$ for gas
c_T	Total gas concentration (mol/m^3)
c_{eq}	Equilibrium concentration of a gas (mol/m^3)
dp	Average particle diameter (m)
E	Activation energy for rate constant (J/mol)
F	Material flux $(kg/m^2.s)$ for solid
F_p	Product gas flux $(mol/m^2.s)$
F_{v_W}	Volumetric flux of water (m/s)
ΔG^o	Standard free energy change (kJ/mol)
ΔH^o	Standard free enthalpy change (kJ/mol)
h	Height (m)
K	Hydraulic conductivity (m/s)
k_r	Reaction rate constant $(1/s)$
m	Molar fraction (unitless)
M	Molecular weight (kg/mol)
P	pressure (Pa)
Pr	Prandtl no. $(unitless)$
$\hat{Q}$	Heat flux (W/m^2)
q_i	Heat of reactions (J)
R	Universal gas constant $(J/mol.K)$
r	Radius (m)
r_c	Carbon conversion rate (kg/s)
T	Temperature (K)
T^*	Wall heat transfer temperature (K)
t	Time (s)
U	Heat transfer coefficient $(W/m^2.K)$
V	Wall recession velocity (m/s)
W	Mass fraction (unitless)
x_i	Constants which are depending upon the local Reynolds number
z	Cavity Height (m)

Subscripts

a	Ash
c	Carbon
ch	Char
dry	Drying
e	Extinction
f	Failure Condition
g	Gas
g_f	Gasification
inj	Injection
ox	Oxidation
p	Product gas
s	Solid
ω	Wall
v	Vaporization

Greek Letters

α	Steam to oxygen ratio
ρ	Density (kg/m^3)
κ	Permeability (m^2)
δ	Wall layer thickness (m)
λ	Thermal conductivity $(W/m.K)$
μ	Viscosity $(kg/m.s)$
Ω	Gas injection source term
ψ	Function describing location of permeable ash pile surface

References

[1] E. I. A. (US), G. P. Office, International Energy Outlook 2016: With Projections to 2040, Government Printing Office, 2016.

[2] B. E. Outlook, Bp global, 2017 edition.

[3] B. Dubley, Bp statistical review of world energy june 2014, in: World Petroleum Congress, Moscow. Accessed June, Vol. 16, 2013.

[4] A. W. Bhutto, S. Karim, Coal gasification for sustainable development of the energy sector in pakistan, Energy for Sustainable Development 9 (4) (2005) 60–67.

[5] P. Sindh Coal & Energy Department, Government of Sindh, Thar coal fields technical specification, block-v, `http://www.sindhcoal.gos.pk/coal-fields/thar-coalfield/` (2012).

[6] R. Sathre, L. Gustavsson, N. Le Truong, Climate effects of electricity production fuelled by coal, forest slash and municipal solid waste with and without carbon capture, Energy 122 (2017) 711–723.

[7] T. Sarkus, W. Ellis, Environmental impacts of coal production, in: Fossil Fuels: Current Status and Future Directions, World Scientific, 2016, pp. 81–97.

[8] H. Tsui, C.-H. Wu, Operating concept of circulating fluidized bed gasifier from the kinetic point of view, Powder technology 132 (2-3) (2003) 167–183.

[9] R. Heinberg, D. Fridley, The end of cheap coal, Nature 468 (7322) (2010) 367–369.

[10] A. Beath, S. Craig, A. Littleboy, R. Mark, C. Mallett, Underground coal gasification: evaluating environmental barriers, in: CSIRO Exploration and Mining Report, 2004.

[11] L. Yang, J. Liang, L. Yu, Clean coal technology-study on the pilot project experiment of underground coal gasification, Energy 28 (14) (2003) 1445–1460.

[12] D. A. Bell, B. F. Towler, M. Fan, Coal gasification and its applications, William Andrew, 2010.

[13] D. J. Roddy, P. L. Younger, Underground coal gasification with ccs: a pathway to decarbonising industry, Energy & Environmental Science 3 (4) (2010) 400–407.

[14] M. Blinderman, D. N. Saulov, A. Y. Klimenko, Forward and reverse combustion linking in underground coal gasification, Energy 33 (3) (2008) 446–454.

[15] S. J. Friedmann, R. Upadhye, F.-M. Kong, Prospects for underground coal gasification in carbon-constrained world, Energy Procedia 1 (1) (2009) 4551–4557.

[16] A. A. Uppal, Modeling and control of underground coal gasification, Ph.D. thesis, COMSATS Institute of Information Technology, Islamabad, Pakistan (2016).

[17] A. A. Uppal, A. I. Bhatti, E. Aamir, R. Samar, S. A. Khan, Control oriented modeling and optimization of one dimensional packed bed model of underground coal gasification, Journal of Process Control 24 (1) (2014) 269–277.

[18] A. A. Uppal, A. I. Bhatti, E. Aamir, R. Samar, S. A. Khan, Optimization and control of one dimensional packed bed model of underground coal gasification, Journal of Process Control 35 (2015) 11–20.

[19] A. A. Uppal, Y. M. Alsmadi, V. I. Utkin, A. I. Bhatti, S. A. Khan, Sliding mode control of underground coal gasification energy conversion process, IEEE Transactions on Control Systems Technology 26 (2) (2018) 587–598.

[20] A. Jowkar, F. Sereshki, M. Najafi, A new model for evaluation of cavity shape and volume during underground coal gasification process, Energy 148 (2018) 756–765.

[21] G. Perkins, Underground coal gasification–part ii: Fundamental phenomena and modeling, Progress in Energy and Combustion Science 67 (2018) 234–274.

[22] G. Perkins, Mathematical modelling of underground coal gasification, University of New South Wales, 2005.

[23] V. Prabu, S. Jayanti, Simulation of cavity formation in underground coal gasification using bore hole combustion experiments, Energy 36 (10) (2011) 5854–5864.

[24] J. Britten, C. Thorsness, A model for cavity growth and resource recovery during underground coal gasification, Tech. rep., Lawrence Livermore National Laboratory, CA (USA), UCRL-99987, (1988).

[25] D. W. Camp, A review of underground coal gasification research and development in the united states, Tech. rep., Lawrence Livermore National Lab.(LLNL), Livermore, CA (USA) (2017).

[26] E. Biezen, J. Bruining, J. Molenaar, et al., An integrated 3d model for underground coal gasification, in: SPE annual technical conference and exhibition, Society of Petroleum Engineers, 1995.

[27] M. Najafi, S. M. E. Jalali, R. KhaloKakaie, F. Forouhandeh, Prediction of cavity growth rate during underground coal gasification using multiple regression analysis, International Journal of Coal Science & Technology 2 (4) (2015) 318–324.

[28] G. Samdani, P. Aghalayam, A. Ganesh, R. Sapru, B. Lohar, S. Mahajani, A process model for underground coal gasification–part-i: Cavity growth, Fuel 181 (2016) 690–703.

[29] G. Samdani, P. Aghalayam, A. Ganesh, R. Sapru, B. Lohar, S. Mahajani, A process model for underground coal gasification–part-ii growth of outflow channel, Fuel 181 (2016) 587–599.

[30] D. Camp, J. Nitao, J. White, G. Burton, C. Reid, J. Friedmann, A fully integrated 3-d multi-physics ucg simulator applied to ucg field tests, in: A presentation at the 2nd IEA Underground Coal Gasification Network Workshop, Banff, Alberta, Canada, 2012.

[31] S. Daggupati, R. N. Mandapati, S. M. Mahajani, A. Ganesh, A. Pal, R. Sharma, P. Aghalayam, Compartment modeling for flow characterization of underground coal gasification cavity, Industrial & Engineering Chemistry Research 50 (1) (2010) 277–290.

[32] G. Perkins, V. Sahajwalla, A numerical study of the effects of operating conditions and coal properties on cavity growth in underground coal gasification, Energy & Fuels 20 (2) (2006) 596–608.

[33] S. Daggupati, R. N. Mandapati, S. M. Mahajani, A. Ganesh, D. Mathur, R. Sharma, P. Aghalayam, Laboratory studies on combustion cavity growth in lignite coal blocks in the context of underground coal gasification, Energy 35 (6) (2010) 2374–2386.

[34] V. Prabu, S. Jayanti, Laboratory scale studies on simulated underground coal gasification of high ash coals for carbon-neutral power generation, Energy 46 (1) (2012) 351–358.

[35] G. Perkins, Underground coal gasification–part i: Field demonstrations and process performance, Progress in Energy and Combustion Science 67 (2018) 158–187.

[36] M. S. Blinderman, A. Y. Klimenko, Underground Coal Gasification and Combustion, Woodhead Publishing, 2017.

[37] C. Thorsness, J. Britten, Lawrence livermore national laboratory underground coal gasification project:final report, Tech. rep., Lawrence Livermore National Laboratory, CA (USA), UCID-21853 (1989).

[38] J. Britten, C. Thorsness, A mechanistic model for axisymmetric cavity growth during underground coal gasification, Am. Chem. Soc 33 (1988) 126–133.

[39] J. Britten, C. Thorsness, Further development of an axisymmetric global ucg cavity growth simulator, Tech. rep., Lawrence Livermore National Laboratory, CA (USA), UCRL-96461 (1987).

[40] J. Britten, C. Thorsness, A mechanistic model for axisymmetric ucg cavity growth, Tech. rep., Lawrence Livermore National Laboratory, CA (USA), UCRL-94419 (1986).

[41] C. Thorsness, J. Britten, Cavism user manual, Tech. rep., Lawrence Livermore National Laboratory, CA (USA), UCID-21667 (1989).

[42] A. Edward, C. Thorsness, Unconfined flow as a mechanism of water influx to a ucg system, Tech. rep., Lawrence Livermore National Laboratory, CA (USA), UCRL-97203 (1987).

[43] E. A. Grens, C. Thorsness, Wall recession rates in cavity growth modeling, Tech. rep., Lawrence Livermore National Laboratory, CA (USA), UCRL-90729 (1985).

[44] E. A. Grens, C. Thorsness, The effect of nonuniform bed properties on cavity wall recession, Tech. rep., Lawrence Livermore National Laboratory, CA (USA), UCRL-92487 (1986).

[45] E. A. Grens, C. Thorsness, Modeling thermal and material interactions between a reacting char bed and a gasifying/spalling coal roaf, Tech. rep., Lawrence Livermore National Laboratory, CA (USA), UCRL-92488 (1985).

[46] I. Khurshid, M. A. S. Baig, J. Choe, et al., Utilization of coal deposits of thar colliers with underground coal gasification, opportunities and challenges in syngas generation, in: SPE/PAPG Annual Technical Conference, Society of Petroleum Engineers, 2013.

[47] A. A. Memon, S. A. Shaikh, H. Mahar, M. Uqaili, S. Hussain, A. Palari, T. Ashraf, Undergroud coal gasification and utilization of syngas in various fields, Journal of Faculty of Engineering & Technology 23 (1) (2016) 75–85.

[48] C. Thorsness, S. Kang, A method-of-line approach to solution of packed-bed flow problems related to undergound coal gasification processs, Tech. rep., Lawrence Livermore National Laboratory, CA (USA), (1984).

[49] M. Field, D. Gill, W. Hawksley, Combustion of pulverized coal, Cheney & Sons Ltd., 1967.

[50] R. Govind, J. Shah, Modeling and simulation of an entrained flow coal gasifier, AIChE Journal 30 (1) (1984) 79–92.

[51] J. Bear, Dynamics of Fluids in Porous Media, American Elsevier , New York, Ch.8, 1972.

[52] A. C. Hindmarsh, Lsode and lsodi, two new initial value ordinary differential equation solvers, ACM Signum Newsletter 15 (4) (1980) 10–11.

[53] C. G. Broyden, A class of methods for solving nonlinear simultaneous equations, Mathematics of computation 19 (92) (1965) 577–593.

[54] G. EUROPE, Gas 3100 r coal gas/syngas 19-3u analyser, Gas Engineering and Instrumentation Technologies Europe, Bunsbeek, Belgium.

[55] M. Imran, D. Kumar, N. Kumar, A. Qayyum, A. Saeed, M. S. Bhatti, Environmental concerns of underground coal gasification, Renewable and Sustainable Energy Reviews 31 (2014) 600–610.

[56] A. N. Khadse, M. Qayyumi, S. M. Mahajani, P. Aghalayam, Reactor model for the underground coal gasification (ucg) channel, International Journal of Chemical Reactor Engineering 4 (1).

[57] O. G. Oyugi, B. Gathitu, H. Ndiritu, A review on the effect of feed oxygen, water concentration, temperature and pressure on gasification proce, in: Proceedings of Sustainable Research and Innovation Conference, 2017, pp. 134–139.

[58] A. Hamanaka, F.-q. Su, K.-i. Itakura, K. Takahashi, J.-i. Kodama, G. Deguchi, Effect of injection flow rate on product gas quality in underground coal gasification (ucg) based on laboratory scale experiment: development of co-axial ucg system, Energies 10 (2) (2017) 238.

[59] G. Samdani, P. Aghalayam, A. Ganesh, S. Mahajani, A process model for underground coal gasification–part-iii: Parametric studies and ucg process performance, Fuel 234 (2018) 392–405.

LaTeX Source Files

Click here to download LaTeX Source Files: Latx Files.zip